Aerodynamics and rain rivulet suppression of bridge cables with concave fillets

Celeste Burlina[*1], Christos T. Georgakis[2b], Søren V. Larsen[3c] and Philipp Egger[4d]

[1]*Technical University of Denmark, Copenhagen, Denmark*
[2]*Aarhus University, Aarhus, Denmark*
[3]*FORCE Technology, Copenhagen, Denmark*
[4]*VSL International Ltd., Bern, Switzerland*

Abstract. In this paper, the aerodynamic performance of two new cable surfaces with concave fillets (strakes) is examined and compared to plain, dimpled and helically filleted surfaces. To this end, an extensive wind-tunnel campaign was undertaken. Different samples with different concave fillet heights for both new surfaces were tested and compared to traditional surfaces in terms of aerodynamic forces (i.e. drag and lift reduction) and rain-rivulet suppression. Furthermore, flow visualization tests were performed to investigate the flow separation mechanism induced by the presence of the concave fillet and its relation to the aerodynamic forces. Both new cable surfaces outperformed the traditional surfaces in terms of rain-rivulet suppression thanks to the ability of the concave shape of the fillet to act as a ramp for the incoming rain-rivulet. Furthermore, both new surfaces with the lowest tested fillet height were found to have drag coefficients in the supercritical Reynolds range that compare favorably to existing cable surfaces, with an early suppression of vortex shedding.

Keywords: cable aerodynamics; concave fillets; rain rivulet suppression; flow visualization; static forces

1. Introduction

Worldwide economic development has led to a significant increase in long-span bridge construction. The reduced cost and ease of construction of cable stayed bridges has made them the choice bridge for medium to longer spans.

Cable-stayed bridges have been constructed in past with a variety of different types of cable, but the parallel mono-strand cable has emerged as the preferred solution in recent years, for reasons of cost, maintenance, and corrosion protection (Gimsing and Georgakis 2012).

The parallel mono-strand cable employs three layers of corrosion protection, namely galvanization of the wires, a polyethylene wrap of the individual strands and a final outer HDPE (High Density Polyethylene) sleeve for all of the strands. The outer casing is traditionally circular in shape, the aerodynamic performance of which has been extensively studied.

In earlier applications, smooth-surfaced cables were often employed. This surface, generally stable with respect to wind action under dry conditions, can become very unstable under the combination of rain and wind. In certain conditions, the rainwater forms small rivulets, which flow down the surface of the cable and make the apparent cable cross-section aerodynamically unstable. The resulting vibration phenomenon is called rain-wind induced vibration (RWIV). RWIV can reach amplitudes as high as a several diameters of the cable, and therefore pose a significant threat to the fatigue lifetime and serviceability of the structure.

RWIVs constitute 95% of all knows bridge cable vibrations (Gimsing and Georgakis 2012). The mechanism was first identified the late 80's on the Meiko-Nishi Bridge in Japan, during its construction (Hikami and Shairaishi 1988). After this first report, it has become clear that many other cable vibration episodes that had been observed earlier and since for other bridges, can be classified as rain-wind induced vibrations.

Intensive efforts have been made to investigate the mechanism of RWIV and to provide appropriate vibration control measures, which come mainly in three forms: the placement of dampers between the cables and the bridge girder, cross-ties between the cables, and aerodynamic control which results from manipulation of the cable section shape and surface (Hojo *et al.* 2000).

Several different aerodynamic cable surfaces have been proposed to date in order to control vibrations either through prevention of rain-rivulet formation or by disturbing the flow around the cable. Two cable surfaces currently dominate the market, namely helical fillets, which are extensively used in Europe and North America, and dimples, which are used predominantly in Asia (Fig. 1). Nevertheless, the introduction of helical fillets and dimples has not completely eliminated RWIVs, often leading bridge

*Corresponding author, Ph.D. Student
 E-mail: celebur@byg.dtu.dk
[a] Professor
 E-mail: cg@eng.au.dk
[b] Ph.D.
 E-mail: svl@force.dk
[c] Ph.D.
 E-mail: philipp.egger@vsl.com

Helically Filleted Surface   **Dimpled Surface**

Fig. 1 Cable sample models from previous aerodynamic measures

HC fillted surface   **HSC filleted surface**
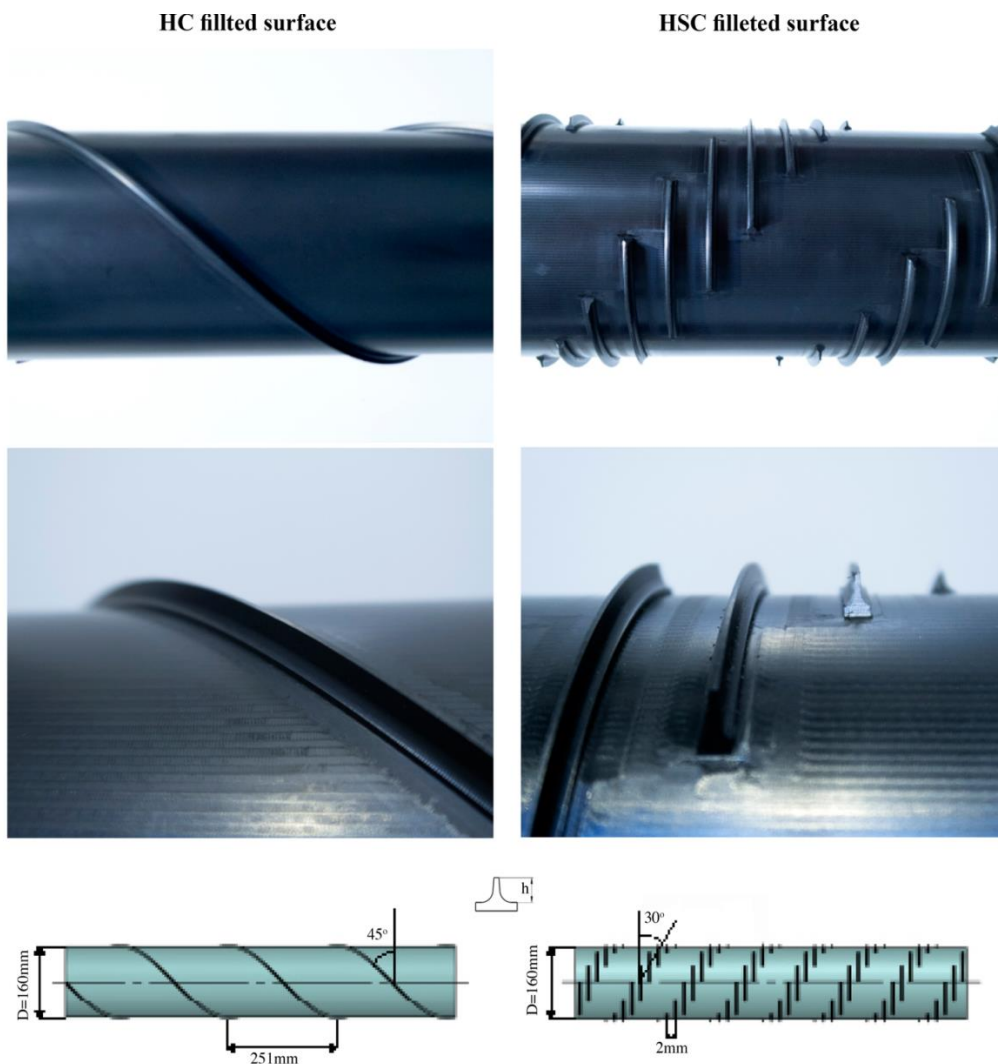
Fig. 2 Cable sample models with concave fillets

owners to install cable vibration dampers or cross-ties. Previous research (Yagi 2011, Kleissl and Georgakis 2013) shows that by modifying the shape, alignment and configuration of the protuberances on the HDPE tube, it is possible to eliminate or further reduce the RWIVs, together with a reduction in drag force.

In particular, preliminary investigations of cable surface modifications involving concave fillets, as undertaken by Kleissl and Georgakis (2013), were found to outperform traditional surfaces, showing similar aerodynamic force coefficients, compared to traditionally helically filleted and dimpled surfaces despite a significant increase in the fillet height.
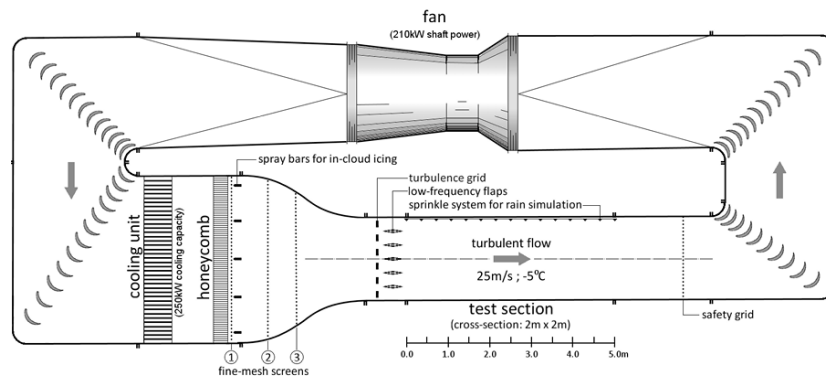
Fig. 3 Climatic wind tunnel at FORCE Technology, Denmark
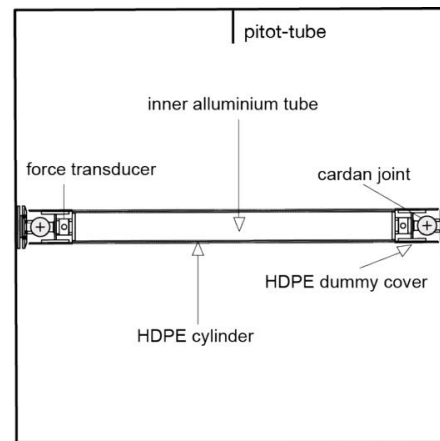
Fig. 4 Normal flow test set-up

As a result, the objective of the present work is to further examine the aerodynamic performance and understand the behavior of innovative bridge cable surfaces with concave fillets, particularly when compared with plain, dimpled and helically filleted surfaces. Focus is placed on the determination of the flow structure and development of the near-wake of bridge cables, so as to make it possible to adjust and thus improve concave fillets for the purpose of drag reduction, while at the same time guaranteeing optimal rain-rivulet suppression. To this end, an extensive wind-tunnel test campaign was performed at the Climatic Wind Tunnel (CWT) at FORCE Technology (Denmark). Different samples with varying concave fillet heights were tested and compared to the traditional surfaces in terms of aerodynamic forces and rain-rivulet suppression. Furthermore, flow visualization tests were performed to investigate the flow separation mechanism induced by the presence of the different fillet shapes. This investigation allows for the understanding of the dependencies of the height and the radius of the concave fillet on the suppression of the rain-rivulet and on the development of the wake in relation to the resultant drag and lift coefficients.

2. Sectional models

The models tested were full-scale samples of high density polyethylene (HDPE) tubing. As mentioned, several cable surfaces were tested for the purpose of comparison (Fig. 2). These included a plain surface cable, a traditional helically filleted cable, a dimpled cable, a helically concave (HC) filleted surface and a helically staggered concave (HSC) filleted surface. The plain HDPE tube has a 160 mm outer diameter. The HDPE tubes with two helically wrapped fillets also have an outer diameter of 160 mm. The fillets are rounded with a height of approximately 2 mm on the first sample and 4 mm on the second sample, with a pitch angle of 45° and a spiral distance of 251 mm. The pattern-indented tube has a diameter of 140 mm, as this is an actual sample of the most common diameter of cable used on the Sutong Bridge. The relative surface roughness is defined by the depth of the indentations, measured to be approximately 1% of cable diameter. The surface with concave fillets were first proposed by Kleissl and Georgakis (2013) and have two major mechanical functions. Firstly, the fillets work as a ramp for rain rivulets, forcing water to leave the surface of the cable. Secondly, the concave sides

and the sharp tip of the fillet lead to stronger directional guidance of the remaining water along the fillet (Kleissl and Georgakis 2013). For helically concave filleted surface, the fillets replicate the typical arrangement of current stay cables with helical fillets, which results in a 45° pitch angle and a spiral distance of 251 mm.

For the helically staggered concave filleted surface, the fillets are arranged laterally in a staggered helical pattern with a pitch angle of 30° and spacing between the fillets of 20 mm.

For both concave filleted surfaces, three different heights of the fillet were produced and tested in order to understand the dependency of the height and arrangement of the fillet on the drag force and its ability to maintain optimal performance in terms of rain-rivulet suppression. In the original design first proposed by Kleissl and Georgakis (2013), a height (h) of 6.9 mm (h/D = 0.043) was used. From the original design, two additional fillet heights were chosen for testing. For the HC filleted surface, the height was set at 4.3mm (h/D = 0.027) and 5.3 mm (h/D = 0.033). For the HSC filleted surface, the height was set at 4.3 mm (h/D = 0.027) and 8.9 mm (h/D = 0.055). The tallest fillet, for HSC filleted surface, was chosen after considerations about the possible advantages during ice and snow events, as it could lead to a greater accretion retention.

3. Experimental work

3.1 Wind tunnel facility

The closed-circuit climatic wind tunnel has a test chamber cross-section of 2 m x 2 m and is 5 m long, which allows for testing of full-scale cables sections, with a diameter up to approximately 200 mm in cross-flow, that would equate to a maximum blockage ratio of 10%. The tests were performed at a temperature of approximately 20°C. Wind velocities up to 31 m/s can be generated with an average turbulence intensity of less than 1% in normal conditions, i.e., without turbulence grids or the water spray system mounted. The wind velocity was measured with a Pitot-static tube, which was mounted on the ceiling mid-width of the test chamber's cross-section and placed 1.5 m upstream of the tested models. Turbulence intensity was found to be in range of I_u=0.7% to 1.1% for varying wind velocities, with a value of 0.9% for the average wind velocity of 20 m/s.

3.2 Normal flow test set up

The cables section prototypes were placed horizontally in the wind-tunnel cross section, resulting in a near two-dimensional flow normal to the cable section. The set up was made as rigid as possible for the execution of the static tests. The drag and lift forces were measured using 6 DOF force transducers (AMTI MC3A-500) placed at either end. The two force transducers were installed between the cable model and supporting cardan joints. The cardan joints were installed in order to reduce the bending moments on the force transducers and to align the cable between the two

side walls of the wind tunnel cross-section. The transducers and the joints were covered with dummy pieces of the same cable material and diameter. A gap of approximately 2 mm was left between the cable model and the dummy pieces. The HDPE tube and the inner alluminium tube were fixed by means of through-screws in order to avoid any relative movement.

The length of the models was 1.52 m, resulting in an aspect ratio of 8.9:1. The blockage ratio for the cable model was 8% and thus the drag coefficients have been corrected using the Maskell III method, according to Cooper *et al.* (1999).

During the tests the wind velocity was increased by regular increments of approximately 1 m/s within a range of 5 to 30 m/s, allowing for supercritical Reynolds numbers to be reached for all tested repetitions. The time window used in all measurements was 30 s and the sampling frequency was 2048 Hz.

For each tested configuration, the drag C_D and the lift C_L coefficients were calculated, based on the averaged along-wind and across-wind forces respectively, normalized by the along-wind flow velocity

$$C_D = \frac{F_D}{\frac{1}{2}\rho U^2 LD} \tag{1}$$

$$C_L = \frac{F_L}{\frac{1}{2}\rho U^2 LD} \tag{2}$$

where F_D is the total along-wind force and F_L is the across-wind component, U is the mean wind, L is the effective length of the cable, D the outer diameter of a plain surface cable, without taking into consideration cable surface modifications and ρ the air density, taken here as 1.25 kg/m³.

3.3 Flow visualization

During the flow visualization tests, cable samples were placed normal to the flow for comparison with the results obtained from the static tests. Smoke particles were added to the flow to trace the fluid motion. In order to visualize a slice of the fluid flow pattern, the particles were illuminated with a sheet of laser light. With smoke particle sizes in the order of 0.2 µm, it can be assumed that the particles faithfully follow the streamlines of the flow (Kleissl *et al.* 2013). For this, a high-output smoke generator was employed using a water-based quick dispersing smoke fluid. The smoke injection was applied approximately 0.5 m upwind of the cable samples. Due to dispersion of the particles at high wind velocities, tests were run up to the sub-critical Reynolds number range limit, namely Re ≈ 0.6 x10⁵. The laser sheet was generated with a green (532 nm) 3W continuous-wave diode-pumped solid-state laser and a 451 Powell lens line generator ensuring a uniform intensity throughout the sheet. The laser sheet had a thickness of approximately 2 mm.
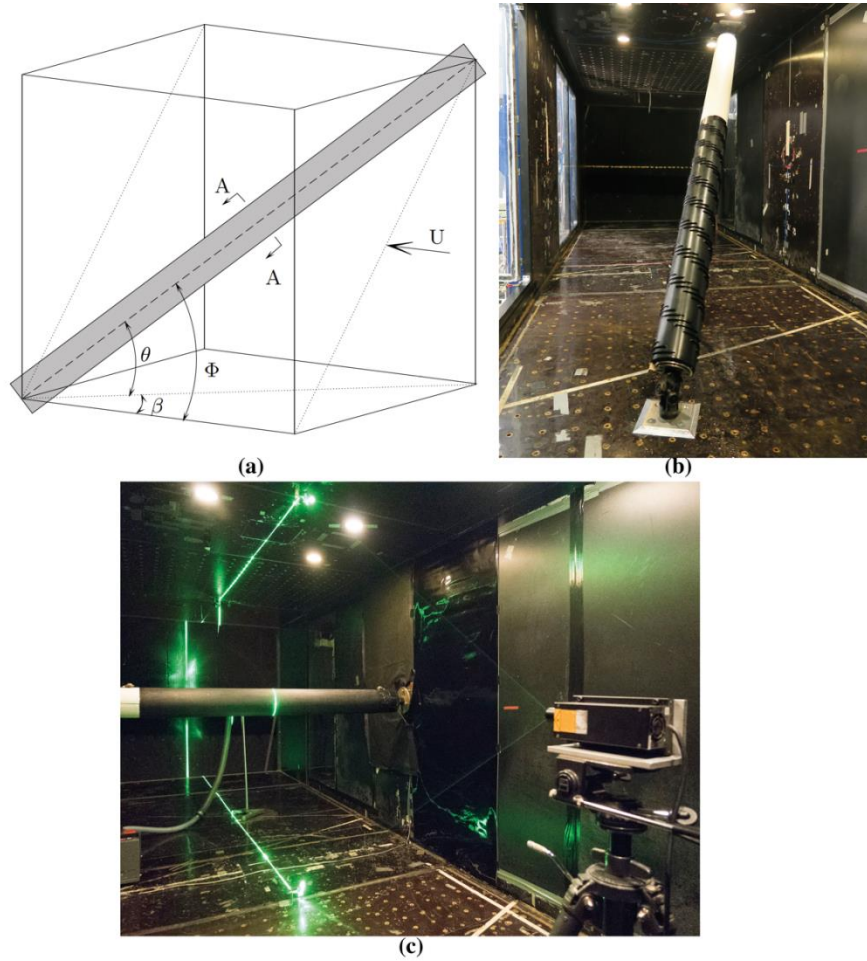
Fig. 5 Rain-wind induced vibration set-up schematics (a), rivulet suppression set-up (b) and flow visualization set-up (c)

3.4 Rain rivulet suppression

Rivulet suppression tests were performed with the cable declining along the wind direction. The inclination is quantified through the wind-cylinder angle, ϕ, i.e., the angle between the mean flow and the cylinder axis. When gravity affects the behaviour (e.g., in presence of water or ice accretions on the cylinder surface) or when the cylinder is not perfectly symmetric, two angles must be considered: the yaw angle, β, i.e., the angle between the projections of the mean flow and the cylinder axis in the horizontal plane, and the inclination angle, Θ, i.e., the angle between the cylinder axis and the horizontal plane. The relationship between ϕ; β and Θ is

$$\phi = arcos(cos\Theta cos\beta) \qquad (1)$$

In the current set-up tests were performed at a cable inclination angle of $\Theta = 40^{\circ}$ and with a yaw angle of $\beta = \pm 22.5^{\circ}$, resulting in a relative cable-wind angle of $\phi = 45^{\circ}$ (Kleissl and Georgakis 2013). A plain surface cable section was used to make up the first top half of the model length, in order to facilitate the formation of the upper and lower rivulet, while varying cable sections were used to make up the second half of the length. Kick-starting the rivulet on the first plain surface half of the model allowed for an easy evaluation of the distance the rivulets could travel along the modified cable section before complete suppression (Kleissl and Georgakis 2013). All tests were repeated for 7m/s (Re = 7.06 x 10^4) and 15m/s, (Re = 1.63 x 10^5) which are the representative values for the lower and upper velocity range for RWIVs respectively.

4. Results and discussion

4.1 Rain rivulet suppression

The formation of one or two rain water rivulets (upper and/or lower) and the rivulet motion as well, is a necessity for the development of large amplitude vibrations (see e.g., Hikami and Shiraishi 1988, Flammand 1995, Cosentino *et al.* 2003, Yamauchi *et al.* 2008, Kleissl 2013). The formation of the upper rivulet requires relatively moderate wind speeds. The upper rivulet forms on the side of the cable where the wind hits the cable surface, because the wind prevents the water from sliding down. Therefore, the wind speed cannot be too high, as this would blow the water to the other side of the cable where gravity will lead it down. On the other hand, the wind speed cannot be too low, as the water would slide down and join the lower rivulet.

Helically Filleted Surface - h/D=0.0125

Helically Filleted Surface - h/D=0.025
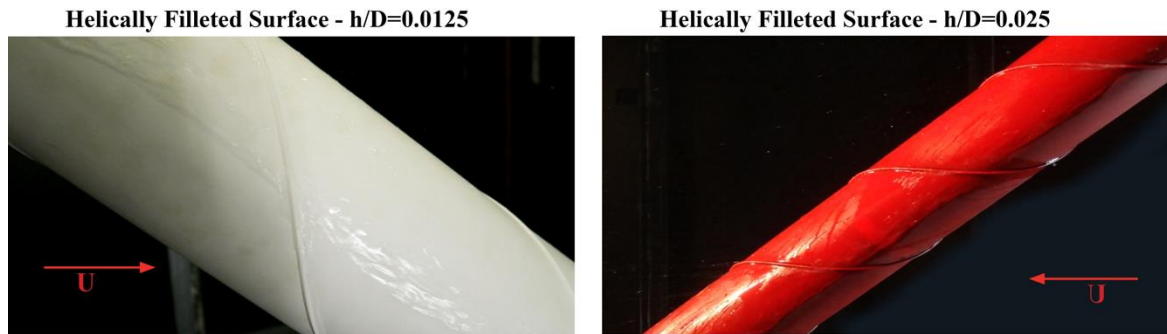
Fig. 6 Rain rivulet suppression of traditionally helically filleted surfaces

HC filleted surface - h/D=0.043

HSC filleted surface - h/D=0.043
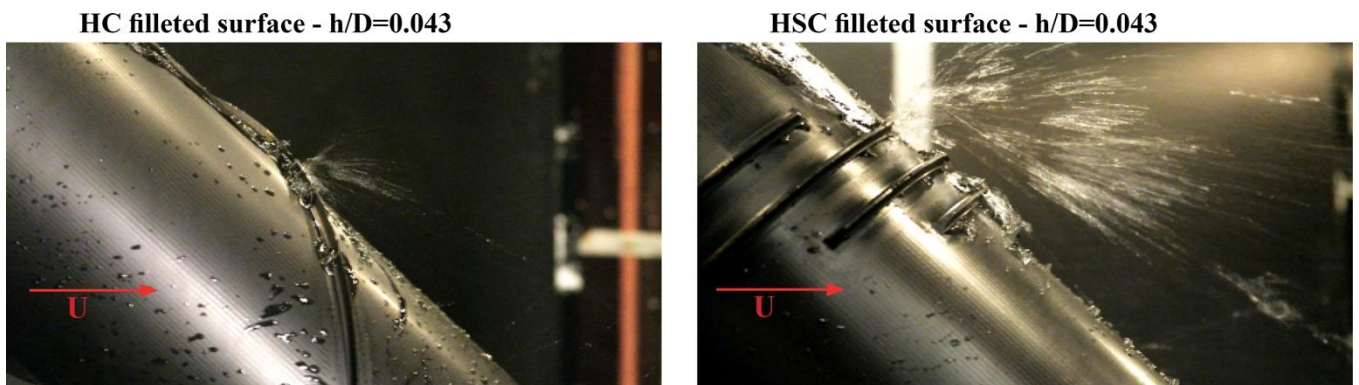
Fig. 7 Rain rivulet suppression of helically concave filleted surfaces

The structural conditions and weather conditions for RWIVs to take place on a smooth cable surface have been compiled over the years, Gimsing and Georgakis (2012), and widely researched by Hikami and Shiraishi. (1988), Matsumoto *et al*. (1992), Flamand *et al*. (1995), Larose *et al*. (1999), Cosentino *et al.* (2003), although not all are in accordance. The general conditions include wind speeds between 7 - 15 m/s, cable frequencies 0.5-3.3 Hz, yaw angles 0-45° (0° being parallel to the cable axis), light to moderate rainfall of around 1-10 mm/h, low wind turbulence and mainly stays declining along the wind. Since the oscillations of the rivulets were seen as the driving parameter by these researchers, it is thought to either suppress or disorganise the rivulet movement, while keeping aerodynamic forces, in particular the drag coefficient, at an acceptable level. After studies were carried out, the helical fillet and pattern-indented surface has been mainly applied to the protective tubes of stay cables. Recent studies performed by Yamauchi *et al.* (2008), show that a disorganization of the rain-rivulet should be sufficient to suppress RWIV.

Nevertheless, these modifications are not fully able to supress vibrations. Rain-wind induced vibrations were reported on studies on the Øresund Bridge for the traditional helically filleted cable (Larose and Smitt 1999, Acampora and Georgakis 2011) and on studies regarding the pattern-indented cables on bridges (Chen 2011, Katsuchi 2011) and in wind tunnel tests (Katsuchi and Yamada 2011). Due to such discoveries and since vibrations in dry weather conditions also have been observed for

cables with helical fillets (Christiansen *et al.* 2015), other surface treatments have been preliminary tested by Kleissl (2013) to prevent vibrations in dry and wet conditions. Test were run statically up to the post-critical regime (Re=3.5 x 10^5) and dynamically in a Reynolds number range from 0 up to 2 x 10^5 on the HC and HSC filleted surface with a fillet height of h/D=0.043. The results from the wet dynamic tests show that neither of the two new innovative surfaces were found to suffer from RWIV when tested dynamically. In dry conditions one of the innovations with helically arranged strakes was observed to experience the same limited amplitude vibrations as observed for other cables with helical fillets. On the other hand, the innovative cable with staggered concave strakes was dynamically stable in dry conditions (Kleissl 2013).

A parametric investigation is herewith performed on the concave filleted cable sections in order to understand the dependencies of the variation of the concave fillet height in terms of rain rivulet suppression, since the complete removal of the rivulet will totally eliminate the mechanism leading to RWIV. Comparison also is made with traditional cable surfaces with similar fillet height in order to understand the influence of the fillet shape on the formation and/or suppression of the rain rivulet. Furthermore, by lowering the concave fillet height from the original height tested by Kleissl (2013), better aerodynamic performances can be achieved. Fig. 6 shows the rain rivulet suppression ability of the tested cable surfaces. The helically filleted surface for both the different fillet heights of h/D=0.0125 and h/D=0.025 is able to reduce the size of the rain rivulet

Upper Rivulet

h/D=0.043   h/D=0.033   h/D=0.027

Lower Rivulet

h/D=0.043   h/D=0.033   h/D=0.027
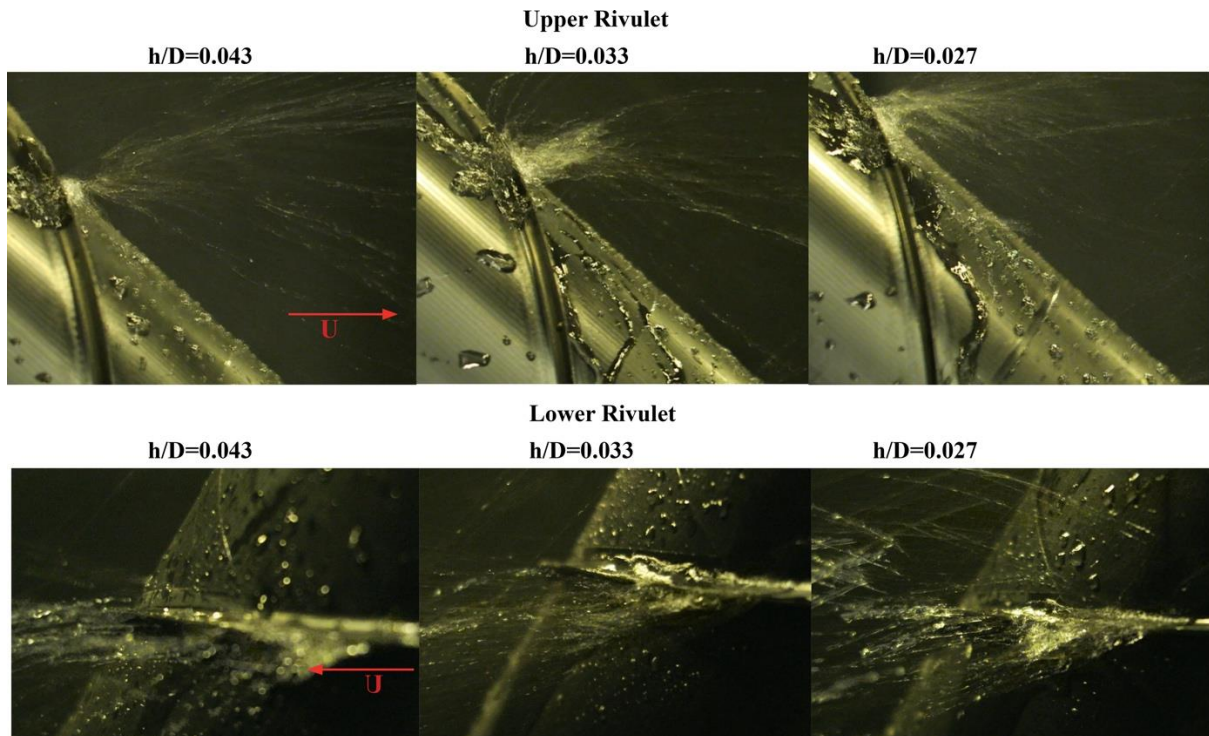
Fig. 8 Rain rivulet suppression for different concave fillets heights

along the length of the cable and the way the rain-rivulet is formed but it is not able to completely suppress it. These observations are in agreement with recent tests performed by Yamauchi *et al.* (2008) on cable with double helical ribs with a fillet height of h/D=0.014. Results from the wet dynamic tests on the sample show a similar disorganized rain-rivulet running on the cable surface. On the other hand, concave filleted cables experience a complete suppression of the upper and lower rivulets at both wind velocities tested (Fig. 7).

The particular shape of the concave fillet acts as a ramp, blocking the formation of the upper and lower rivulet along the whole length of the cable. It was noted that this is mainly due to the concavity of the fillet and its sharp top edge (Burlina *et al.* 2016). Furthermore, and unlike the traditional cables, the concave fillet is able to supress upper and lower rivulet formation, even with the lowest tested height of h/D=0.027 (Fig. 8).

Regarding the dimpled surface, it was not possible to test the sample due to rain rivulet suppression test set-up constraints. From previous studies performed by Kleissl and Georgakis (2013), the dimpled surface performs similarly to the traditional helical fillet, which is able to reduce the size of the rain rivulet along the length of the cable but it is not able to completely suppress it.

4.2 Force coefficients

A parametric investigation was performed in cross-flow on the concave filleted cable sections in order to understand the dependencies of the variation of the concave fillet height in terms of aerodynamic forces. Furthermore, they

were compared with the plain, dimpled and traditional helically filleted surfaces under the same conditions.

It can be noted in Fig. 9(a) that for the HC filleted surface there is gradual transition from the sub-critical to the post-critical regime starting from a value of approximately 1.0 to an end value of approximately 0.7 remaining nearly constant after entering the post-critical regime. An accentuated transition in correspondence of the critical Reynolds number does not appear as for the plain cable surface (see Zdravkovich 1986).

Fig. 9(a) also shows the variations of drag coefficient with the Reynolds number for the three different heights of concave fillet (h/D = 0.027, 0.033 and 0.043). Note a decrease of the drag coefficients in the supercritical range from 0.76 down to 0.71 with the decrease of the fillet height from 6.9 mm to 4.3 mm.

As a result, there is a clear dependency of the fillet height on the level of drag force while showing the same transitional behaviour from the sub-critical to the post-critical regime. The difference can be attributed to form drag.

When compared to a helically filleted surface (Fig. 9(c)), the HC filleted surface with the 4.3 mm concave fillet height experiences the same drag force compared to the traditional helical fillet with a 4 mm fillet height. The helically filleted surface with the 2 mm fillet height experiences a lower drag of 0.64 when entering the post-critical range. This is due to a more accentuated drag transition in the Reynolds number range between 2.0 and 2.6 x 10^5.
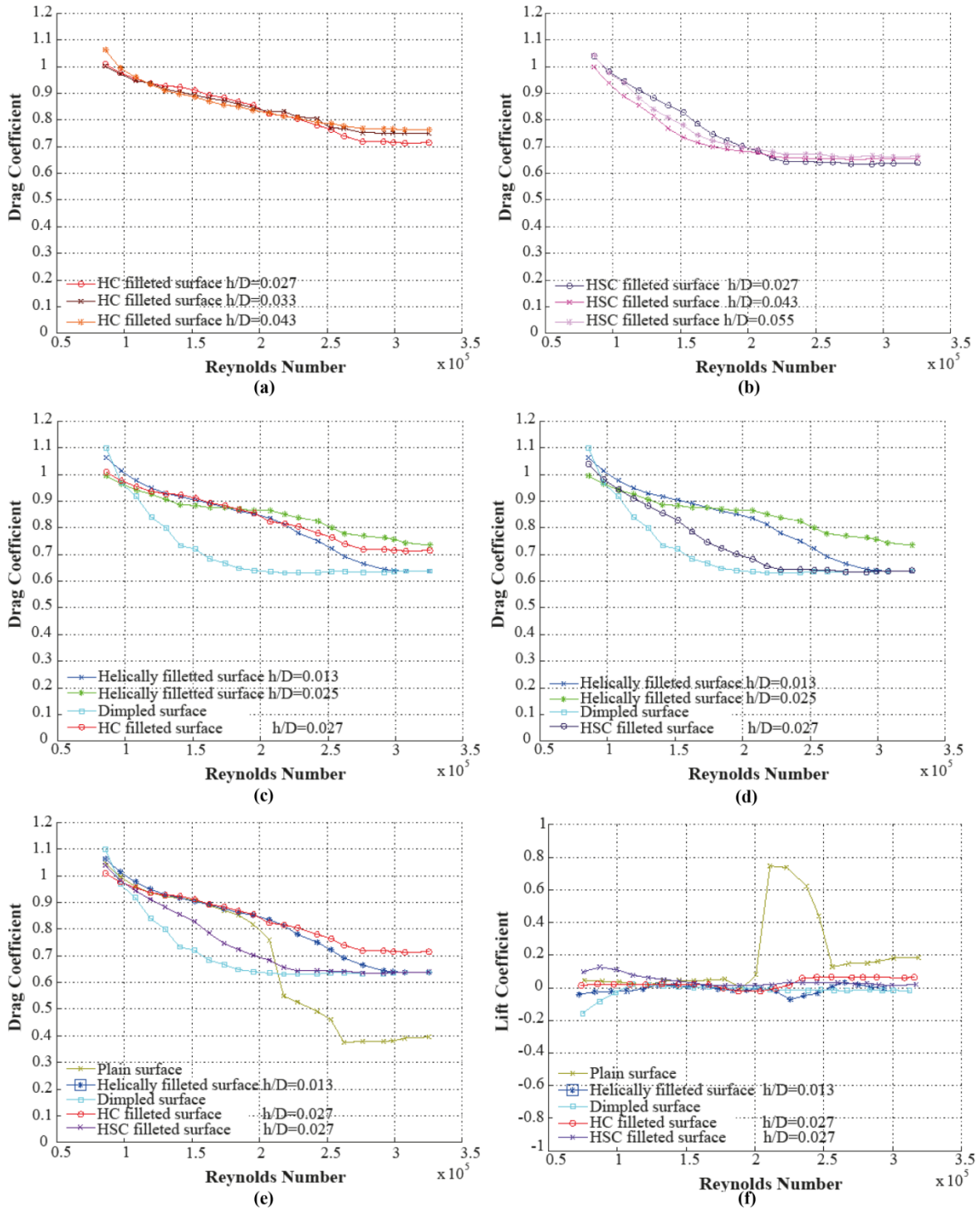
Fig. 9 Force coefficients

Despite the same arrangement of the fillet for the surfaces in question, the higher drag coefficient in the post-critical Reynolds range for the HC filleted surface cable can be attributed to the higher profile and concave shape of the fillet directly facing the incoming flow, which acts as a fixed ramp and separation point and thus resulting in a wider wake. As was noted from Fig. 7(a), this phenomenon is reduced when the concave fillet height is reduced (Burlina *et al.* 2016). Different heights of concave fillet (h/D = 0.027, 0.033 and 0.043). Note a decrease of the drag coefficients in the supercritical range from 0.76 down to 0.71 with the decrease of the fillet height from 6.9 mm to 4.3 mm.

Plain surface

Helically filleted surface h/D=0.025

Dimpled surface
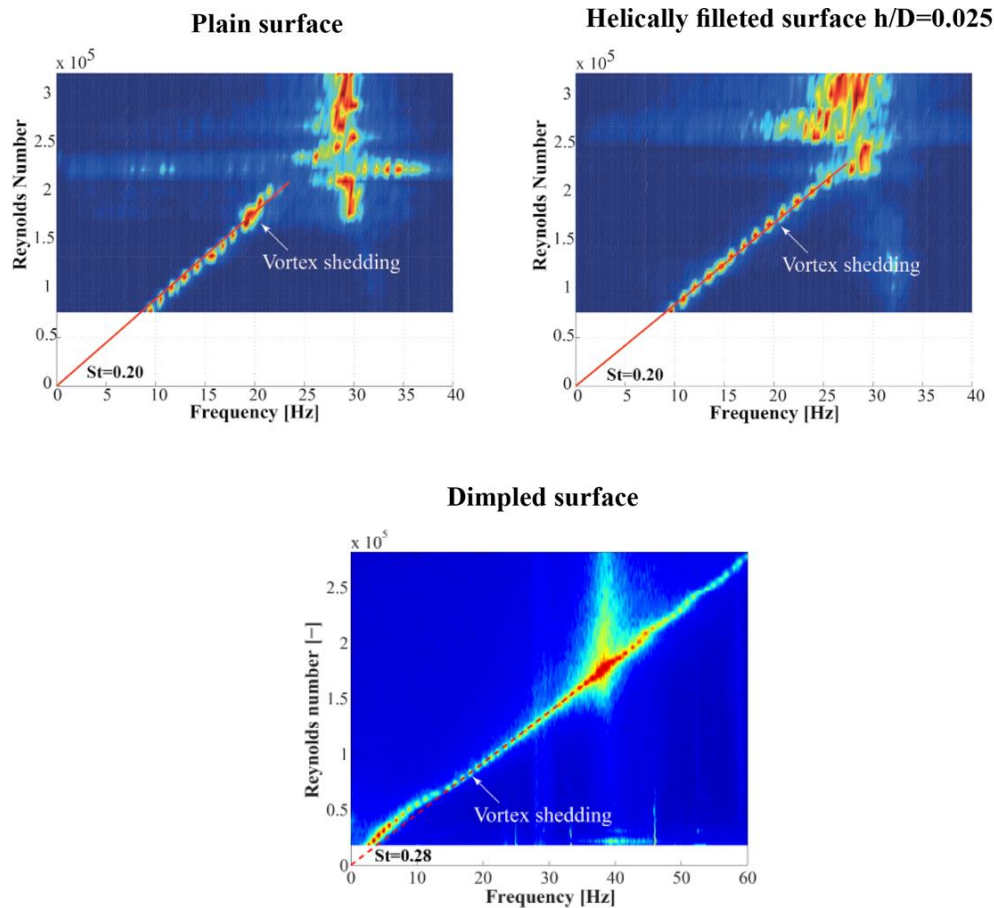
Fig. 10 Power spectral density (PSD) of lift coefficients for traditional cable surfaces

As a result, there is a clear dependency of the fillet height on the level of drag force in the post-critical regime. A higher fillet creates localized wider wake, influencing the overall level of drag force, not allowing for a boundary layer transition, narrowing of the wake and subsequent decrease in drag force. The same transitional behaviour from the sub-critical to the post-critical regime is noticed for all fillets heights tested. The difference can be attributed to form drag.

When compared to a helically filleted surface (Fig. 9(c)), the HC filleted surface with the 4.3 mm concave fillet height experiences the same drag force compared to the traditional helical fillet with a 4 mm fillet height. The helically filleted surface with the 2 mm fillet height experiences a lower drag of 0.64 when entering the post-critical range. This is due to a more accentuated drag transition in the Reynolds number range between 2.0 and 2.6×10^5. Despite the same arrangement of the fillet for the surfaces in question, the higher drag coefficient in the post-critical Reynolds range for the HC filleted surface cable can be attributed to the higher profile and concave shape of the fillet directly facing the incoming flow, which acts as a fixed ramp and separation point and thus resulting in a wider wake. As was noted from Fig. 7(a), this phenomenon is reduced when the concave fillet height is reduced (Burlina *et al.* 2016).

The HSC filleted surface (Fig. 9(b)) exhibits an earlier reduction in the drag force in the sub-critical Reynolds range and a smooth and prolonged flow transition which starts at lower Reynolds numbers between $0.8 - 1.0 \times 10^5$. The flow enters a post-critical state at a Reynolds number of about 2.0×10^5 with a constant drag force value of about 0.65. This behavior results in near constant drag coefficients over a wide range of Reynolds numbers, after the initial reduction.

The drag coefficient (Fig. 9(b)) of approximately 0.65 is maintained, when either increasing the concave fillet height up to 8.3 mm (h/D = 0.055) or decreasing it down to 4.3 mm (h/D = 0.027). As stated earlier, it is believed, that this optimal performance is due to the ability of the staggered sharp shaped concave fillet facing the flow, and the circumferential orientation, to enhance vorticities at the boundary layer resulting in a turbulent boundary layer flow. A turbulent boundary layer flow has a larger momentum than laminar boundary layer flow, thus resulting in a delayed flow separation and in a narrower wake. This leads to the subsequent lower drag.

When comparing drag, the HSC filleted surface and the dimpled surface show a similar behavior over the tested Reynolds number range. On the other hand, the HSC filleted surface shows a smoother transition compared to the dimpled surface, leading to lower risk of aerodynamic
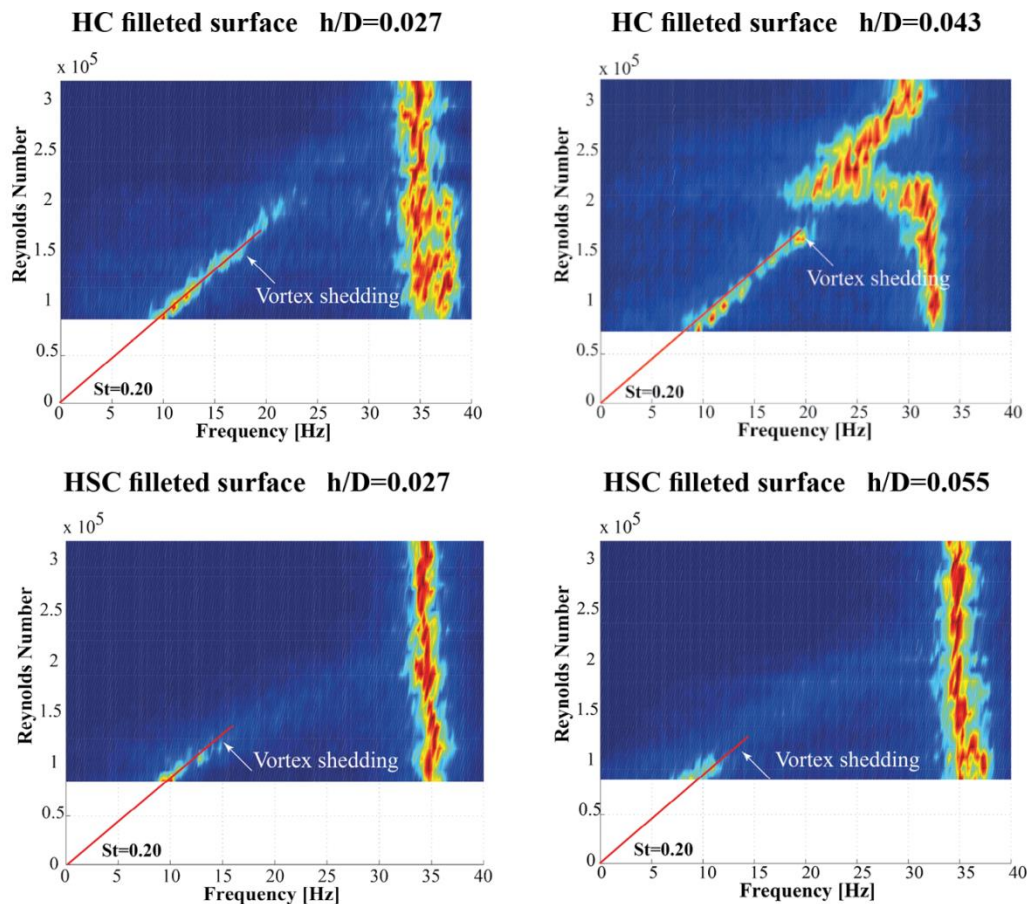
Fig. 11 Normal flow lift coefficients (PSD) for helically concave filleted cable surfaces

instabilities over the affected Reynolds numbers interval. The early flow transition for the dimpled surface cable agrees well with what has been observed for circular cylinders with uniform high roughness, which easily triggers turbulence ensuring a near constant super-critical drag (Miyata *et al.* 1994, Hojo *et al.* 1995).

Concerning the lift force, apart from the plain cable surface, the other four cable surfaces experience an almost zero lift along the whole range of wind velocities tested (Fig. 9(f)). This is most likely due to the ability of all the surface modifications to generate variations in the flow and separation lines along the length of the cable. These variations, as largely reported in previous studies, are the result of enhanced vorticities and counter rotating vortices for the dimpled surface (Miyata *et al.* 1994) and of periodic structures in the spanwise direction with localized increased streamwise vorticities and elongations of the vortex formation region for the traditional helical fillet (Nebres and Batill 1993). It must be noted that recent studies by Larose *et al.* (2012) and Matteoni *et al.* (2013) show a sensitivity of the aerodynamic performance of the cables, with both plain and helically filleted surfaces, with respect to the cable wind angle of attack. This is due to the deviation of the cable from its original circular shape. The studies show that each time the cable was rotated on its axis, a new shape was exposed to the flow and a different behaviour can be expected in terms of lift force.

4.3 Fluctuating lift forces

A frequency analysis of the unsteady cross-stream force (fluctuating lift) is undertaken. With the particular cross flow test set up employed, the fluctuations of the total lift force on the model can be determined. The frequency distributions of the lift force are determined using a Fast Fourier Transformation (FFT) to compute the power spectral density (PSD) of the lift coefficient. The PSD is computed for each of the flow velocities tested. The discrete number of flow velocity-specific spectra is then expanded into a two-dimensional contour plot, as seen in Figs. 10 and 11, for each of the cable models. The Strouhal number is computed for all five cables ($St = f_s\, D/U$, where f_s is the frequency of vortex shedding). The increased PSDs at around 30 and 35 Hz can be explained as the incidences of model resonance.

The linear trend, identifying vortex shedding, disappears around a Reynolds number between 2.0 and 2.2 x 10^5 for the plain cable and the traditional helically filleted cable respectively. These values correspond for both surfaces to the flow transition from the sub-critical to the post-critical Reynolds number regions. The same linear behavior disappears at much lower Reynolds numbers for the cable surfaces with the concave fillet for the whole range of fillet heights tested. This occurs at Reynolds number around 1.5 x 10^5 for both concave filleted surfaces, which corresponds
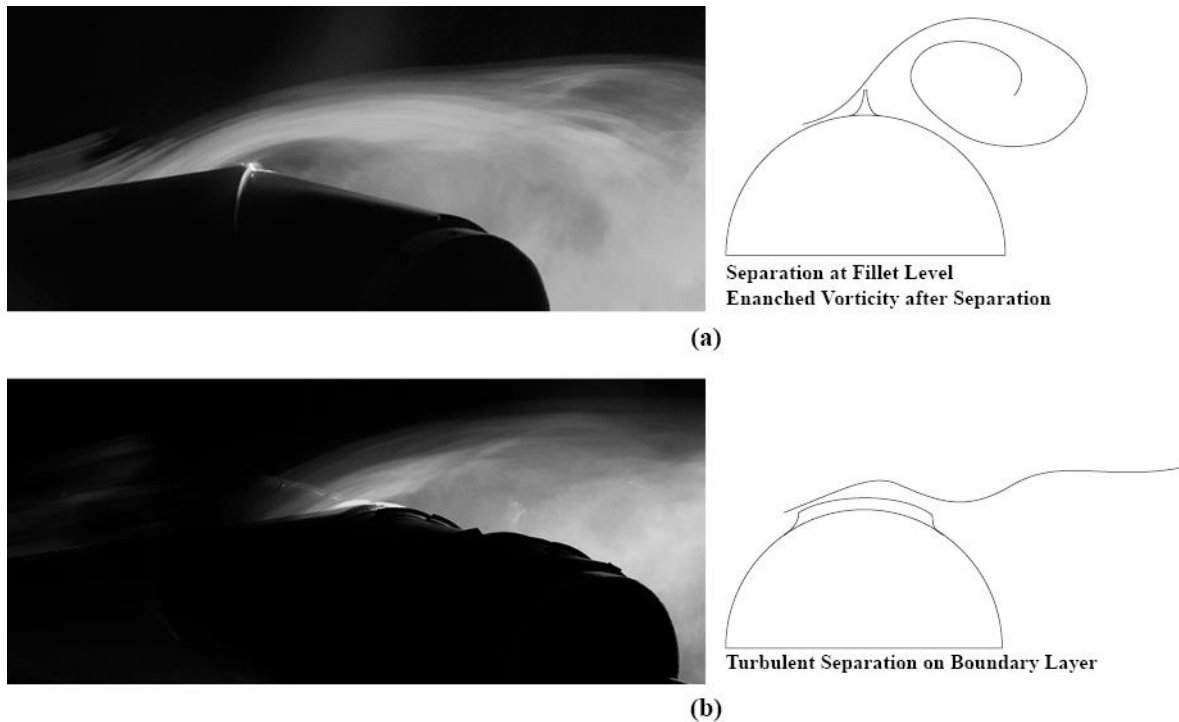
Fig. 12 Flow separation mechanism for HC filleted surface (a) and HSC filleted surface (b)

to the smooth and prolonged drag transition for the HC filleted surface and to the entrance in the super-critical regime for the HSC filleted surface. On the other hand, the vortex shedding remains throughout the whole range of tested velocities for the dimpled cable surface, despite the early flow transition at a Re = 0.8-1.0 x 10^5, as experienced also by the HSC filleted surface. Furthermore, a significantly higher Strouhal number of 0.28 is determined for the dimpled surface compared to the other samples, which were founded to have a Strouhal number of 0.20. As a result, both concave filleted surfaces are able to suppress vortex shedding formation at much lower wind velocities than a traditional helically filleted or dimpled surface. The HSC filleted surface, which experiences the same drag reduction showed by the dimpled surface, is able to suppress vortex shedding in the same range as the transition to the super-critical regime.

4.4 Flow visualization tests

Flow visualization tests were performed on the HC filleted and the HSC filleted cable surfaces for the varying concave fillet heights. The aim of the tests was to understand the disturbance created by the concave fillet on the incoming flow, the separation mechanism, and subsequent development of the near wake.

Figs. 12(a) and (b) shows the separation points created by the concave fillet in both cables at the subcritical Reynolds number of 0.6 x 10^5. The concave fillet in the HC filleted surface (Fig. 12(a)), is seen as a solid fence to the oncoming boundary layer flow. In this way, it creates a fixed separation point and a subsequent recirculating zone behind the concave fillet. Hence, as the concave fillet height

is increased from 4.3 mm (h/D = 0.027) to 6.9 mm (h/D = 0.043), a larger recirculation zone is formed behind the fillet. As a result, the height of the fillet changes the aerodynamic performance of the cable with a dependency on the diameter of the cable in terms of h/D ratio. In fact, the increase in size of the recirculating zone created behind the fillet will affect the possibility for early flow reattachment, a delayed further downstream turbulent separation, and a narrower wake. This particular behavior does not allow for a transition in the flow for increased Reynolds numbers, which would lead to a reduction of the wake´s size and subsequently a reduction of the drag coefficient in the supercritical range (See Fig. 9).

On the other hand, the same concave fillet applied in a helical staggered configuration (HSC filleted surface) shows a different separation mechanism (Fig. 12(b)). The concave fillets are oriented parallel to the flow, so that the fillet cross section is perpendicular to the flow, leading them to behave as vortex generators. Vortex generators are small plates, in the form of wedges, fences, fairing, etc., mounted to a surface, so as to protrude into the flow. They work by generating a strong overturning macro-vortical motion of the near-wall flow (Gad-El-Hak and Bushnell 1991) causing high energy air outside the boundary layer to be fed into the lower energy region within the boundary layer and thus, through mixing enhancement, results in an enhanced momentum in the vicinity of the wall. In this particular case, it is believed that the large velocity differences generate a region of high shear, resulting in the formation of a pair of counter-rotating vortices. These pairs of vortices leak larger-scale streamwise vorticity into the wake, which stabilizes the narrow wake provided by the delayed separation.

HC filleted surface - h/D=0.0.043 (6.9mm fillet)
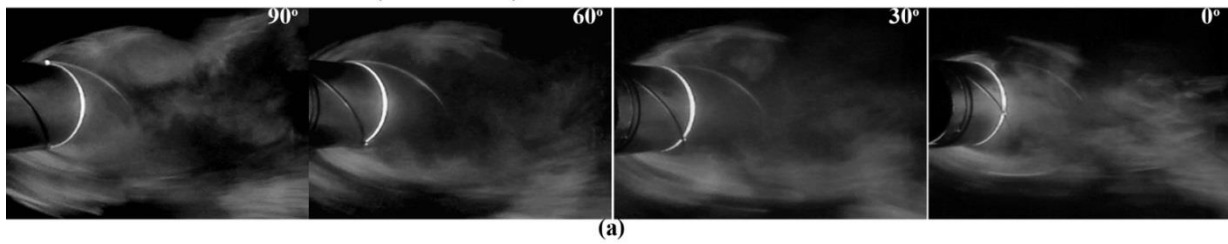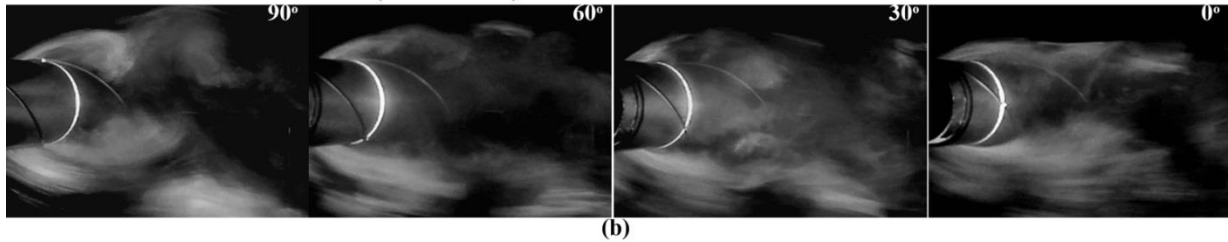
(a)

HC filleted surface - h/D=0.0.027 (4.3mm fillet)

(b)

HSC filleted surface - h/D=0.0.055 (8.3mm fillet)

(c)

HSC filleted surface - h/D=0.0.027 (4.3mm fillet)

(d)
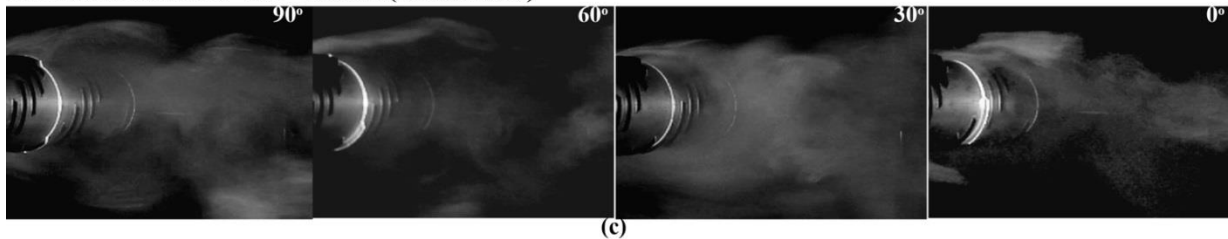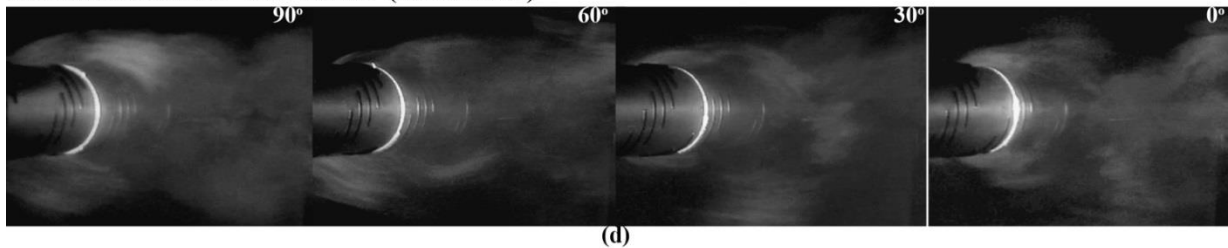
Fig. 13 Near wake development

This is the major cause of an earlier transition to the supercritical region with a steady low drag force of approximately 0.65 (See Fig. 13). By increasing the fillet height from 4.3 mm (h/D = 0.027) to 8.9 mm (h/D = 0.055) the same behavior is observed. This is due to the high sharp edge of the concave fillet, which does not affect the flow separation mechanism. As a result, the same level of drag is maintained over the whole range of Reynolds number tested for the different fillet height.

In Fig. 13, the development of the near wake for varying angular positions (0°, 30°, 60°, 90°) for both helically concave filleted surfaces and for the two lower and taller fillets is shown. Different angular positions are achieved by rotating the cable around its axis starting from a fillet position directly facing the flow at 90°.

Through this, it is possible to understand the influence of the fillet height and of the helical orientation on the eneration of three-dimensional flow structures, as they create uncorrelated fluctuations along the span of the cylinder (Zdravkovich 1981, Nebres and Batill 1993).

In the case of the HC filleted surface, the different angular position of the concave fillet along the spanwise direction creates various flow regimes and separation mechanisms as identified by Nebres and Batill (1993), Ekmekci and Rockwell (2010). When arranged helically, the axial overlap of these mechanisms results in a periodic waviness in the separation line and wake width as illustrated in Fig. 13. Furthermore, when considering different concave fillet heights, the development of the tridimensional structure of the wake is enhanced (h/D = 0.043) or reduced (h/D = 0.027) resulting in a higher or lower drag force.

In the case of HSC filleted surface, the helical orientation of the staggered fillets creates a spanwise phase mismatch in the vortex-shedding process. As a result, the vortical structure becomes three-dimensional and loses its strength. The larger near-wake width created by the fillet positioned at 90° in respect to the incoming flow, retard the

interaction between the vortices shed from the upper and lower edge on the cable. This mechanism creates an area of acceleration and suction along the spanwise of the cable (Park *et al.* 2006). It is believed that the low drag that characterizes the HSC filleted surface is not only due to the turbulent separation generated by the fillet as previously explained, but also by the three-dimensional flow created by the vortex dislocation in the wake, resulting in a mean-velocity modification along the spanwise direction (acceleration and deceleration) and in a narrower wake. Furthermore, as the separation mechanism is not influenced by the fillet height, the wake development and resulting drag force are not affected.

5. Conclusions

Two new cable surfaces with concave fillets are wind tunnel tested for the determination of the aerodynamic coefficients, the structure of the flow´s near-wake and for rain-rivulet suppression. The results are compared with traditional cables with plain, dimpled and helically filleted surfaces.

Furthermore, a parametric investigation is performed on the concave fillet shape in order to evaluate its performance when applied on both helically concave filleted surfaces.

The helically concave filleted surfaces outperformed the traditional cable surfaces in terms of rain-rivulet suppression, with a complete suppression of the upper and lower rain-rivulets at all tested velocities. This is true even for the profile with the shortest concave fillet tested. This is due to the ability of the concave fillet to act as a ramp for the incoming rain-rivulet.

The helically staggered concave filleted surface exhibits the same behaviour as a dimpled cable surface in terms of drag coefficient, showing an early transition to the supercritical range and a subsequent reduction of the drag force. This is due to the ability of the staggered surface configuration to enhance turbulence at the boundary layer level. The HSC filleted surface is also able to suppress vortex shedding formation at lower Reynolds numbers, unlike the dimpled cable surface, which maintains it up to the critical Reynolds number range (Burlina *et al.* 2016). Furthermore, the HSC filleted surface is able to maintain a low level of drag even with an increase of the height of the concave fillet from its original design, which represents a more than 100% increase of the fillet height compared to a traditional helical fillet.

The helically concave filleted surface shows a higher drag in the super-critical range compared to HSC filleted surface. This is due to the helical arrangement of the concave fillet, which acts as a fixed ramp and separation point and thus resulting in a wider wake. This phenomenon is reduced with a reduction of the height of the fillet.

References

Acampora, A. and Georgakis, C.T. (2011), "Recent monitoring of the Ø resun Bridge: Rain-wind induced cable vibrations", *Proceedings of the 13th International Wind Engineering Conference*, Amsterdam.

Burlina, C., Georgakis, C.T., Larsen, S.V. and Egger, P. (2016), "Comparative analysis of bridge cables with concave fillets", *Proceedings of the 1st International Symposium on Flutter and its Application (ISFA2016)*, Tokyo, Japan.

Burlina, C., Georgakis, C.T., Larsen, S.V. and Egger, P. (2016), "Optimization of bridge cables with concave fillets", *Proceedings of the 8th International Colloquium on Bluff Body Aerodynamics and Applications (BBAA VIII)*, Boston, USA.

CBC News, British Columbia (2012). "Port Mann Bridge closure unacceptable, says minister", http://www.cbc.ca/news/canada/british-columbia/story/2012/12/20/bc-port-mann-ice.html (Dec. 20, 2012)

Chen, Z.Q. (2011), Hunan University, Jul 2011. Cable vibration incidence of the Jintang Bridge, private communications.

Choi, H., Jeon, W. and Kim, J. (2008), "Control of flow over a bluff body", *Annu. Rev. Fluid Mech.*, **40**, 113-139.

Choi, J., Jeon, W. and Choi, H. (2006), "Mechanism of drag reduction by dimples on a sphere", *AIP Phys. Fluid.*, **18**, 041702.

Christiansen, H., Jakobsen, J.B., Macdonald, J.H.G., Larose, G.L and, Bosch, H.R. (2015), "Aerodynamics of stay cable with helical fillets – Part I: stability and load characteristics", In: preprint submitted Journal of Wind Eng. Ind. Aerodyn.

Cooper, K., Mercke, E. and Wiedemann, J. (1999), "Improved blockage corrections for bluff-bodies in closed and open wind tunnels", *Proceedings of the 10th International Conference Wind Engineering*, Copenhagen, June.

Coesentino, N., Flamand, O. and Ceccoli, C. (2003), "Rain–wind-induced vibration of inclined stay cables. Part I: experimental investigation and physical explanation", *Wind Struct.*, **6**(6), 471-484.

Ekmekci, A. and Rockwell, D. (2010), "Effects of a geometrical surface disturbance on flow past a circular cylinder: a large-scale spanwise flow", *J. Fluid Mech.*, **665**, 120-157.

Flamand, O. (1995), "Rain-wind induced vibration of cable", *J. Wind Eng. Ind. Aerod.*, **57**(2-3), 353-340.

Flamand, O. and Boujard, O. (2009), "A comparison between dry cylinder galloping and rain-wind induced excitation", *Proceeding of the 5th European & African Conference on Wind Engineering*, Florence.

Georgakis, C.T., Koss, H.H. and Ricciardelli, F. (2009), "Design specifications for a novel climatic wind tunnel for the testing of structural cables", *Proceedings of the 8th International Symposium on Cable Dynamics*, Paris, France, September.

Gimsing, N.J. and Georgakis, CT. (2012), Cable Supported Bridges Concept and Design, 3rd Ed., John Wiley & Sons Ltd.

Hikami, Y. and Shiraishi, N. (1988), "Rain–wind-induced vibrations of cables in cable stayed bridges", *J. Wind Eng. Ind. Aerod.*, **29**, 409-418.

Hojo, T., Yamazaki, S. and Okada, H. (2000), Development of Lowdrag Aerodynamically Stable Cable with Indented Processing, Nippon Steel Corporation, July (Special Issue on Steel Structure 82), URL /http://www.nsc.co.jp/en/tech/report/pdf/8203.pdfS.

Hojo, T., Yamazaki, S., Miyata, T. and Yamada, H. (1994), "Experimental study on aerodynamic characteristics of cables patterned surfaces", *J. Struct. Eng.*, **40**A.

Hojo, T., Yamazaki, S., Miyata, T. and Yamada, H. (1995), "Development of aerodynamically stable cables for cable-stayed bridges having low resistance", *Bridge. Foundations Eng.*, **6**, 27-32, in Japanese.

Katsuchi, H. (2011), Yokohama National University, Jul 2011. Cable vibration incidence with pattern-indented surface, private communication.

Katsuchi, H. andYamada, H. (2011), Dry galloping characteristics of indented stay cables in turbulent flow. In: 9th International Symposium on Cable Dynamics, Shanghai, China.

Katsuchi, H., Yamada, H., Sasaki, E., Inamori, K. and Kaga, S. (2010), "Study on dry-galloping of inclined cable with real indented surface", *Proceedings of the 21st National Symposium on Wind Engineering*, Japan.

Kleissl, K. and Georgakis, C.T. (2011a), "Comparison of the aerodynamics of bridge cables with helical fillets and a pattern-indented surface in normal flow", *Proceedings of the 13th International Conference on Wind Engineering*, Amsterdam, Netherland.

Kleissl, K. and Georgakis, C.T. (2011b), "Comparison of the aerodynamics of yawed bridge cables with helical fillets and a pattern-indented surface", *Proceedings of the 9th International Symposium on Cable Dynamics*, Shanghai, China.

Kleissl, K. (2013), Cable aerodynamic control. Wind tunnel studies. PhD Thesis. Technical University of Denmark –DTU. Kgs Lyngby, Denmark.

Larose, G.L. and Smitt, L.W. (1999), "Rain/wind induced vibrations of parallel stay cables", *Proceedings of the IABSE Conference*, Sweden.

Matsumoto, M., Shirashi, N. and Shirato, H. (1992), "Rain–wind-induced vibration of cables of cable-stayed bridges", *J. Wind Eng. Ind. Aerod.*, **41-42**, 2011-2022.

Matsumoto, M., Saitoh, T., Kitazawa, M. et al., (1995), "Response characteristics of rain–wind-induced vibration of stay-cables of cable-stayed bridges", *J. Wind Eng. Ind. Aerod.*, **57**, 323-333.

Matsumoto, M. (1998), "Observed behavior of proto type cable vibration and its generation mechanism, In: Bridge Aerodynamics", *Proceedings of the International Symposium on Advances in Bridge Aerodynamics*.

Matsumoto, M., Daito, Y., Kanamura, T., Shigemura, Y., Sakuma, S. and Ishizaki, H. (1998), "Wind-induced vibration of cables of cable-stayed bridges", *J. Wind Eng. Ind.Aerod.*, **74-76**, 1015-1027.

Matteoni, G. and Georgakis, C.T. (2013), "Effects of surface roughness and cross-sectional distortions on the wind-induced response of bridge cables in dry conditions", *Proceedings of the 6th European and African Conference on Wind Engineering*, Cambridge, United Kingdom.

Miyata, Y., Yamada, H. and Hojo, T. (1994), "Experimental study on aerodynamic characteristics of cables with patterned surface", *J. Struct. Eng.*, **40**, 1065-1076.

Miyata, T., Katsuchi, H. and Tamura, Y. (1999), "Comprehensive discussion on structural control for wind-induced responses of bridges and buildings", *Wind Engineering into the 21st Century, Proceedings of the 10th International Conference on Wind Engineering*.

Nebres, J.V. and Batill, S.M. (1992), "Flow about cylinders with helical surface protrusions", 30th AIAA Aerospace Sciences Meeting and Exhibit, Reno, Nevada 92 (0540).

Park, H., Lee, D., Jeon, W., Hahn, S., Kim, J., Choi, J. and Choi, H. (2006), "Drag reduction in flow over a two-dimensional bluff body with a blunt trailing edge using a new passive device", *J. Fluid Mech.*, **563**, 389-414.

Son, K., Choi, J., Jeon, W., Choi, H. (2011), "Mechanism of drag reduction by a surface trip wire on a sphere", *J. Fluid Mech.*, **672**, 411-427.

Yagi, T., Okamoto, K., Skski, I., Koroyasu, H., Liang, Z., Narita, S. and Shirato, H. (2011), "Modification of surface configurations of stay cables for drag force reduction and aerodynamic stabilization", *Proceedings of the 13th International Conference on wind Engineering*, Amsterdam, The Netherlands.

Yamauchi, K., Uejima, H. and Kuroda, S. (2008), "An investigation of the aerodynamic characteristics of cable with surface ribs", *Proceedings of the 6th International Colloquium on Bluff Bodies Aerodynamics and Applications*, Milan, Italy.

Zdravkovich, M.M. (1981), "Review and classification of various aerodynamic and hydrodynamic means for suppressing vortex shedding", *J. Wind Eng. Ind. Aerod.*, **7**(2), 145-189.

Zdravkovich, M.M. (1984), "Reduction of effectiveness of means for suppressing wind-induced oscillation", *Eng. Struct.*, **6**(4), 344-349.

Zdravkovich, M.M. (1997), Flow around circular cylinders vol.1: fundamentals, Oxford Science Publications, 1997.

CC